Optimizing Q-Space Sampling Density for Diffusion Spectrum Imaging

Qiyuan Tian[1], Ariel Rokem[2], Brian L. Edlow[3], Rebecca D. Folkerth[4], and Jennifer A. McNab[5]

[1]*Department of Electrical Engineering, Stanford University, Stanford, CA, United States,* [2]*Department of Psychology, Stanford University, Stanford, CA, United States,* [3]*Department of Neurology, Massachusetts General Hospital, Boston, MA, United States,* [4]*Department of Pathology, Brigham and Women's Hospital, Boston, MA, United States,* [5]*Department of Radiology, Stanford University, Stanford, CA, United States*

Target Audience: Physicists, neuroscientists and clinicians who acquire and analyze diffusion spectrum imaging data.

Introduction: Diffusion spectrum imaging (DSI)[1] leverages the Fourier relationship between the measured q-space diffusion data and the spin-displacement probability density function (PDF) to map complex tissue structures such as crossing fibers. DSI experiments performed with clinical gradient strengths (40-60mT/m) have limited spatial resolution, q-space coverage (q_{max}) and q-space sampling density (Δq). The recent trend towards stronger gradients in clinical scanners[2,3] enables higher q_{max}'s to be achieved in human brains. A higher q_{max} is theoretically beneficial as it increases the spin-displacement resolution. A caveat of using a higher q_{max} is the increased q-space lattice size required to avoid aliasing of the reconstructed diffusion patterns. DSI experiments are lengthy and therefore it is critical to determine the minimum acceptable q-space sampling density in order to minimize scan time. Here we use a novel 3T human MRI scanner[2] equipped with 300 mT/m gradient strength to acquire three DSI datasets, all with the same q_{max} (equivalent to b_{max}=30,000 s/mm^2) but different Δq (17x17x17, 15x15x15 and 11x11x11 Cartesian q-space grids, referred to herein as DSI17, DSI15 and DSI11 respectively), on the same *ex vivo* human brain. These data are used to examine how q-space sampling density affects the fidelity of the voxel-wise orientation distribution functions (ODFs). Specifically, we demonstrate that there is trade-off between ODF sharpness and aliasing artifacts when Δq is insufficient to capture the spin-displacement pattern.

Theory: Generalized q-space imaging2 (GQI2)[4] mathematically combines the Fourier transform and ODFs calculation, analytically deriving a direct relation between the diffusion signal and the ODFs: $ODF(\mathbf{u}) = L_\Delta^3 \int S(\mathbf{q}) H(2\pi L_\Delta \mathbf{q}^* \mathbf{u}) d\mathbf{q}$ and $H(x)=1/3$ $(x=0)$; $2\cos(x)/x^2+(x^2-2)\sin(x)/x^3$ $(x\neq 0)$ where $\mathbf{u}$ is the unit direction in the sphere, $\mathbf{q}$ is the q-space wave vector, S is the DW signal and L_Δ is called sampling length. The ODF represents the proportion of spin displacement along a particular orientation and is computed by integrating the spin-displacement PDF from its center to a sampling distance L_Δ. A lower L_Δ covers only the slow diffusing components and a small range of the PDF resulting in coarser ODFs while a higher L_Δ provides sharper ODFs.

Methods: One whole, fixed human brain (14 hour postmortem interval, 7 months fixation) from a 58 y.o. woman who died of non-neurological causes was obtained with IRB approval. Data were acquired using the MGH–UCLA Connectome scanner (3T MAGNETOM Skyra CONNECTOM, Siemens Healthcare)[2] which consists of a novel AS302 gradient system capable of up to 300 mT/m and 200 T/m/s. A 2D single-refocused SE-EPI diffusion-weighted sequence was used to acquire three data sets (DSI17, DSI15 and DSI11). Acquisition parameters and statistics are listed in Table 1. The datasets were corrected for field drift and eddy current distortions[5] and co-registered using FLIRT[6]. Dipy software[7] was used to compute ODFs.

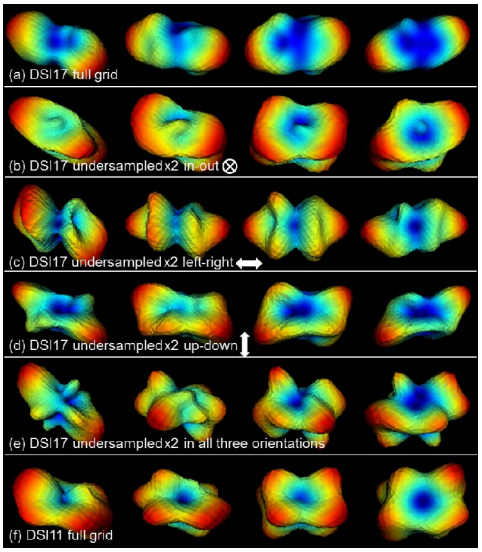

Fig. 1. Aliasing artifacts in ODFs due to the insufficient q-space sampling.

Results and Discussion: Figure 1 displays ODFs from a 1x4 voxel region of interest (ROI) in the center of the corpus callosum (CC) for one fully-sampling (Fig.1a) and four different sub-samplings of the DSI17 data (Fig.1b-e), and for one fully-sampled reconstruction from the DSI11 data (Fig.1f). The ODFs from the full q-grid DSI17 data (Fig.1a) show a clear delineation of the dominant orientation (left-right in Figure 1). When the DS17 data is under-sampled along one orientation at a time (Fig.1b-d) the aliasing along the orientation of under-sampling is clearly visualized. When the DSI17 data is under-sampled along all three orientations simultaneously, the aliasing artifacts (Fig.1e) bear a close resemblance to the ODFs from the fully-sampled DSI11 data (Fig.1f). We infer from this that the fully-sampled DSI11 data is lacking sufficient q-space sampling density to capture the full extent of the spin-displacements. Ultimately, these aliasing artifacts in the under-sampled DSI17 and the fully-sampled DSI11 (Fig.1b-d) obscure the dominant left-right fiber orientation of the CC. In general, the FOV of the spin-displacement PDF, defined by $1/\Delta q$, must be larger than twice the maximum spin displacement that may occur during the experimental diffusion time. Figure 2 displays ODFs, from the right most voxel of the 1x4 ROI shown in Figure 1, reconstructed with different L_Δ. In the top row (Fig. 2a-c), L_Δ is set to the maximum possible spin displacement, i.e. that of free water (18.9μm during the 29.4ms diffusion time used in our experiment). Since most of the diffusion distribution is encompassed within this maximal distance, the resultant ODFs are sharp for the DSI17 and DSI15 data (Fig. 2a-b). For the DSI11 data, the transformed PDFs are aliased due to its narrow PDF FOV. Integrating over the aliased regions leads to abnormal ODFs (Fig. 2c) which are unable to resolve fiber directions. This can be avoided by changing the ODF reconstruction such that L_Δ is limited to half the available PDF FOV (Fig.2f). Unfortunately, this smaller L_Δ distance only covers slow diffusing components resulting in ODFs that are much less sharp and once again the dominant left-right orientation of the CC is lost. ODFs for DSI17 and DSI15 (Fig.2d-e) are similar to those in the top row since the two datasets have large enough PDF FOVs to fully cover the extent of spin displacement.

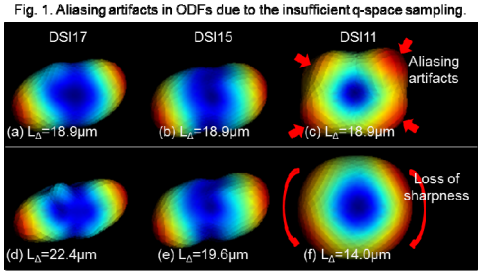

Fig. 2. Trade-off between ODF sharpness and aliasing artifacts.

Conclusion: In order to determine the optimal q-space lattice size that will give sharp ODFs and avoid aliasing artifacts, the spin-displacement FOV ($=1/\Delta q$ or N/q_{max}, where N is the q-grid radius) must be equal to or larger than twice the maximum possible spin displacement. The maximum possible spin displacement is that of free water: $L_{max}=L_{free\_water}=\mathrm{sqrt}(6D_{water}*(\Delta-\delta/3))$, where D_{water} is the diffusion coefficient of free water, Δ is the experimental diffusion time and δ is the duration of one of the diffusion gradient pulses. Therefore N must be equal to or larger than $2xL_{max}xq_{max}$. For our experiments, $N \geq 6.8$ and the optimal N is 7 (i.e. the DSI15 dataset (15x15x15 q-space lattice)). In summary, this study represents an exploration of DSI data with a higher spatial resolution, q_{max} and q-lattice size than has ever before been presented in a human brain. Using this unique dataset, we have developed a method for optimizing q-space sampling density and characterized the ODF artifacts that occur when q-space sampling density is insufficient.

	Δq	PDF FOV	Scan Time	Acquisition Parameters Kept Constant
DSI17	22.3 mm^{-1}	44.8 μm	490 min	G_{max}=252mT/m, b_{max}=30,000 s/mm^2 q_{max}=178.6mm^{-1}, δ/Δ=16.7/29.4ms TE/TR=65/13300ms Spatial FOV=180x138 mm^2 Spatial Resolution=1.5^{3}mm^3, BW=1985 Hz/pixel, GRAPPA R=2, Partial Fourier =6/8
DSI15	25.5 mm^{-1}	39.2 μm	330 min	
DSI11	35.7 mm^{-1}	28.0 μm	120 min	

Table 1. Acquisition parameters and statistics for the three datasets.

Acknowledgments: Funding provided by the Canadian Institute of Health Research, NIH Blueprint for Neuroscience Research Grant, NIH Fellowship: U01MH093765, NIH NCRR P41RR14075 and NIBIB R01EB006847, NEI F32 EY022294.

References: [1] Wedeen VJ et. al. MRM 54(6), 1377-1386, 2005. [2] Setsompop K et. al. NI, 80, 220-233, 2013. [3] Van Essen DC et. al. NI, 80, 62-79, 2013. [4] Yeh F et. al. IEEE TMI, 29(9), 1626-1635, 2010. [5] Bodammer N et. al. MRM, 51(1), 188-193, 2004. [6] Jenkinson M et. al. NI, 62:782-90, 2012. [7] Garyfallidis E et. al. OHBM, 2011.